

Selective Detection of Mg²⁺ for Sensing Applications in Drinking Water

Daniele Paderni,^[a] Eleonora Macedi,^{*,[a]} Larisa Lvova,^{*,[b]} Gianluca Ambrosi,^[a] Mauro Formica,^[a] Luca Giorgi,^[a] Roberto Paolesse,^[b] and Vieri Fusi^{*,[a]}

Abstract: A new series of ligands containing the 2-(2-hydroxy-3-naphthyl)-4-methylbenzoxazole (HNBO) fluorophore showed selectivity for Mg²⁺ ions, without the interference of Ca²⁺. The most promising representative L3 resulted the best

performing sensor for Mg²⁺ both in solution and embedded in an all-solid-state optode, especially towards real samples of drinkable water.

The selective detection of Mg²⁺ in biological and environmental samples arouses great interest in many scientific fields, due to both the crucial role it plays in all living beings as well as the fact that too high or too low levels of Mg²⁺ could be harmful to animals and humans.^[1–3]

Among the analytical procedures able to track Mg²⁺ ions, the employment of optical chemosensors represents an efficient strategy that offers advantages on instrumental methods and rests on simplicity, reliability, velocity and possibility to operate in real time conditions.^[4–10] However, most chemosensors reported so far are not able to distinguish between Mg²⁺ and other metal cations, especially Ca²⁺ and Zn²⁺.^[11–18] The availability of chemosensors that offer selectivity for Mg²⁺ vs. Ca²⁺ thus represents a remarkable analysis tool, both for biological and environmental samples. To this purpose, the development of all-solid-state, disposable and low-cost optical sensors permitting the fast and selective Mg²⁺ detection without the employment of expensive equipment, complex sample preparations and skilled operators involvement is an attractive, as far a challenging analytical task.

Pursuing the aim to develop selective optical chemosensors for Mg²⁺, a new series of ligands containing the 2-(2-hydroxy-3-

naphthyl)-4-methylbenzoxazole (HNBO)^[19] fluorophore linked to different aliphatic amine chains was synthesized (Figure 1).

The series was designed with a growing degree of structural complexity, moving from the simple HNBO to ligands containing one HNBO unit linked to a dimethylamine (N-(2-(2'-hydroxy-3'-naphthyl)benzoxazol-4-ylmethyl)-N,N-dimethylamine, L1) or a N,N,N'-Trimethylethylenediamine fragment (N-(2-(2'-hydroxy-3'-naphthyl)benzoxazol-4-ylmethyl)-N,N',N'-trimethylethylenediamine dihydrochloride, L2·2HCl) or two HNBO units linked to a N,N'-Dimethylethylenediamine fragment (N,N'-bis(2-(2'-hydroxy-3'-naphthyl)benzoxazol-4-ylmethyl)-N,N'-dimethylethylenediamine, L3).

Briefly, ligands L1–L3 were synthesized via a nucleophilic substitution between the amine fragment and the fluorophore, prior bromination at the benzylic position of HNBO (for more details see the Supporting Information, Scheme S1). The latter was previously synthesized as reported in the literature.^[20]

HNBO and the three ligands were mainly tested towards Alkali and Alkaline-earth ions (A and AE in the following; Li⁺, Na⁺, K⁺, Cs⁺, Mg²⁺, Ca²⁺, Sr²⁺, Ba²⁺) in DMSO + 1.5% H₂O solution, at $I = 1.2 \cdot 10^{-3} \text{ mol dm}^{-3}$ NMe₄Cl, and containing an equimolar amount of tetramethylammonium hydroxide (TMAOH) by spectrophotometric and spectrofluorimetric measurements. Among the tested A and AE cations L1–L3 only responded to Mg²⁺, while the sole HNBO fluorophore did not respond to any of them (Figures 2, S1–S4).

[a] Dr. D. Paderni, Dr. E. Macedi, Dr. G. Ambrosi, Prof. M. Formica, Prof. L. Giorgi, Prof. V. Fusi
Department of Pure and Applied Sciences
University of Urbino "Carlo Bo"
Via della Stazione 4, I-61029 Urbino (Italy)
E-mail: eleonora.macedi@uniurb.it
vieri.fusi@uniurb.it

[b] Dr. L. Lvova, Prof. R. Paolesse
Department of Chemical Sciences and Technology
University of Rome "Tor Vergata"
Via della Ricerca Scientifica 1, I-00133, Roma (Italy)
E-mail: larisa.lvova@uniroma2.it

Supporting information for this article is available on the WWW under <https://doi.org/10.1002/chem.202201062>

© 2022 The Authors. Chemistry - A European Journal published by Wiley-VCH GmbH. This is an open access article under the terms of the Creative Commons Attribution License, which permits use, distribution and reproduction in any medium, provided the original work is properly cited.

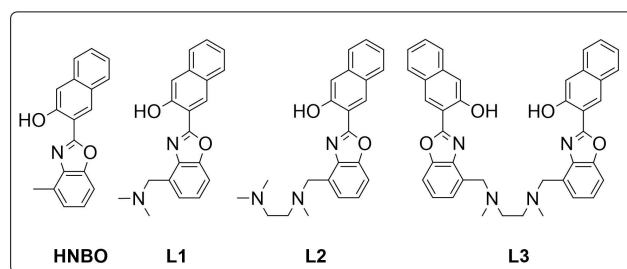


Figure 1. HNBO and HNBO-based ligands L1–L3 synthesized in this study.

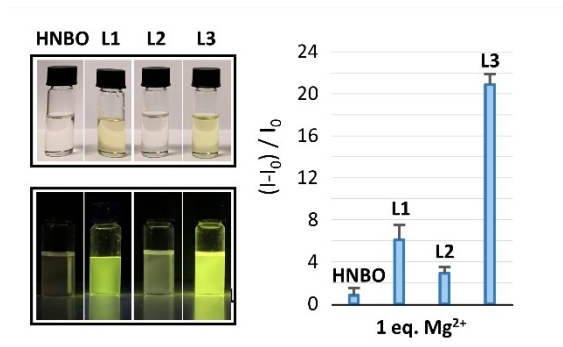


Figure 2. Maximum emission intensity of HNBO and L1-L3 upon addition of 1 equiv. of Mg²⁺ ($\lambda_{\text{ex}} = 440$ nm, $\lambda_{\text{em}} = 530$ nm (HNBO), 540 nm (L1), 535 nm (L2), 537 nm (L3)) and colour change (top) and enhancement of the fluorescence under a 365 nm UV lamp (bottom) after the addition of 1 equiv. of Mg²⁺ to HNBO and L1-L3. [L] = $1.2 \cdot 10^{-5}$ mol dm⁻³ DMSO + 1.5% H₂O; $I = 1.2 \cdot 10^{-3}$ mol dm⁻³ NMe₄Cl. Number of replicas: 3.

Interestingly, among the three ligands L3 showed the highest emission increase in the presence of Mg²⁺, attributed to the coordination of the cation (chelation enhancement of the fluorescence, CHEF effect, Figure 2), considering all A and AE and, noteworthy, some transition metal ions that could possibly interfere in the detection of Mg²⁺ in aqueous medium (Zn²⁺, Cd²⁺ and Pb²⁺; Figures 4a and S5). For this reason, in this contribution the studies performed on L3 are going to be described more in depth.

The UV-Vis absorption titration with Mg²⁺ showed the growth of a new absorption band at 440 nm, ascribable to the deprotonation of the naphthol moiety favored by the coordination of the cation (Figure 3a). The absorption increase parallels the great enhancement of the emission intensity at 537 nm that occurs upon addition of Mg²⁺ ($\Phi = 0.09$ (free ligand), 0.12 (upon addition of 1 equiv. Mg²⁺), $\lambda_{\text{ex}} = 440$ nm, Figure 3b). Both measurements revealed the formation of a species with a 1:1 ligand to Mg²⁺ molar ratio.

¹H NMR titration with Mg²⁺ confirmed the formation of a mononuclear complex, indeed the spectrum did not show any variation following the addition of 1 equiv. of Mg²⁺ (Figure S7). More in detail, moving from the (H₂L3)²⁻ species to the 1:1 complex, all aromatic resonances shift downfield, whereas in

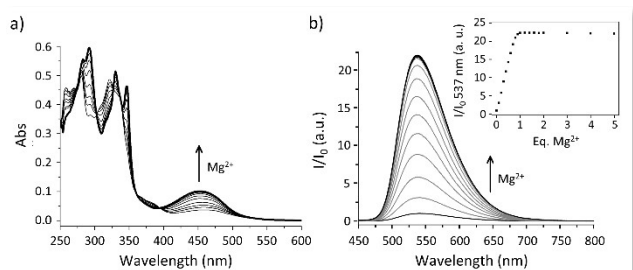


Figure 3. UV-Vis absorption (a) and emission (b) spectra of L3 ($1.2 \cdot 10^{-5}$ mol dm⁻³) in DMSO + 1.5% H₂O, $I = 1.2 \cdot 10^{-3}$ mol dm⁻³ NMe₄Cl upon addition of up to 5 equiv. Mg²⁺. $\lambda_{\text{ex}} = 440$ nm.

the aliphatic region the resonance of H12 shifts upfield and those of H11 and H13 split in characteristic AB systems, suggesting the stiffening of the structure upon the ion complexation (Figure S8). Moreover, since a C₂ symmetry on the NMR time scale is observed, a cooperation between the two fluorophore moieties in the Mg²⁺ complexation can be suggested.

L3 is a possible ESIPT-based sensor:^[21] if this was the case, the metal coordination would suppress the ESIPT mechanism, resulting in an hypsochromically shifted *enol*-fluorescence, and ratiometric signals could be achieved. Since no ratiometric response was observed in this case, another mechanism is to be taken into account. Considering all data and the behavior of L3 at different pH fields (Figure S6), TICT seems to be the prevailing quenching mechanism from acid to neutral pH field, more than PET, while, at basic pH, the deprotonation of HNBO increases the conjugation of the π -system preventing the TICT and PET processes, switching ON the emission. Similarly, the coordination of Mg²⁺ at neutral pH favors the rings conjugation, preventing the TICT and the possible PET quenching^[19,20] affording a highly emitting species (see Supporting Information for more details).

A remarkable fluorescence selectivity of L3 for Mg²⁺ vs. all tested metal ions was observed: among the tested A and AE, only Mg²⁺ caused indeed a pronounced CHEF effect (Figure 4a, blue bars).

The presence in solution of any A and AE did not hamper the fluorescence response of L3 to Mg²⁺, neither individually (Figure 4a, green bars) nor pooled in a solution simulating drinkable water (Figure 4b), indicative of a non-competitive behavior. ¹H NMR measurements revealed an interaction between L3 and Ca²⁺ (generally a strong Mg²⁺ competitor)

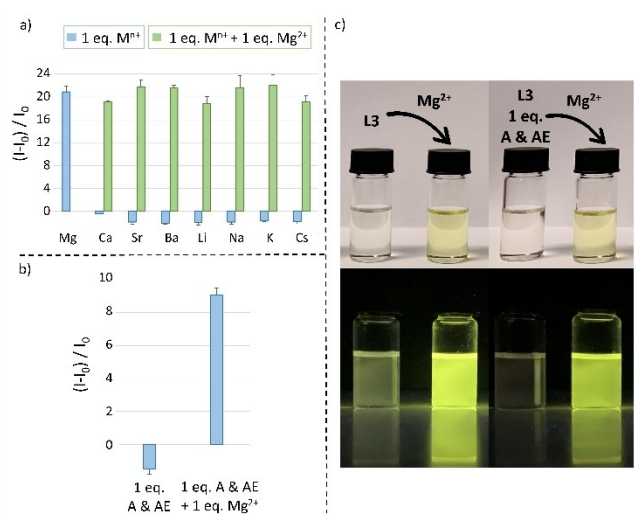


Figure 4. Maximum emission intensity of L3 upon addition of a) 1 equiv. of A and AE or b) an equimolar mixture of A & AE, and following further addition of 1 equiv. of Mg²⁺ ($\lambda_{\text{ex}} = 440$ nm; $\lambda_{\text{em}} = 537$ nm). c) Colour change (top) and enhancement of the fluorescence under a 365 nm UV lamp (bottom) after the addition of 1 equiv. of Mg²⁺ to L3 or an equimolar L3/A & AE mixture. [L3] = $1.2 \cdot 10^{-5}$ mol dm⁻³ DMSO + 1.5% H₂O; $I = 1.2 \cdot 10^{-3}$ mol dm⁻³ NMe₄Cl. Number of replicas: 3.

(Figure S8), but no variation in the emission behavior of the system was observed, as above reported (Figure 4a, blue bars). The addition of Mg^{2+} to the Ca^{2+} -L3 solution switched-ON the emission and produced the ^1H NMR spectrum of the Mg^{2+} -complex (Figure S8), highlighting the better affinity of Mg^{2+} for the chemosensor and the higher stability of the Mg^{2+} -complex compared to the others (Figure 4a, green bars).

The formation of the Mg^{2+} -complex in both the absence and presence of an equimolar A and AE mixture is visible to the naked eye via both a color change of the solution from colorless to yellow as well as a fluorescence increase under a common 365 nm UV lamp (Figure 4c).

The ability of L3 to respond to Mg^{2+} ions in real samples was assessed by analyzing different commercial and tap water samples. To this aim, little amounts of the water samples were added to a DMSO solution of L3, along with distilled water as a comparison. The system proved to work well with the real samples, responding consistently with the Mg^{2+} content of commercial and tap waters (Figure 5), regardless of the complex mixture of cations (including Ca^{2+}) and anions present in solution. Also in this case, the formation of the Mg^{2+} -complex is visible both via colorimetric and fluorimetric change (Figure 5).

The normalized intensity emission at 537 nm of samples doped with Mg^{2+} increased with the Mg^{2+} concentration up to 20 ppm then the system plateaued. The statistical analysis of the trend through the linear regression method^[22] furnished a limit of detection (LOD) of 1.0 ppm ($6.0 \cdot 10^{-7} \text{ mol dm}^{-3}$), a limit of quantification (LOQ) of 3.5 ppm ($2.1 \cdot 10^{-6} \text{ mol dm}^{-3}$) and a limit of linearity (LOL) in the 0–20 ppm range ($1.2 \cdot 10^{-5} \text{ mol dm}^{-3}$) of magnesium ($R=0.99$) (Figure S9).

In light of the promising sensing behavior of L1-L3 in solution, the possibility to develop all-solid-state optodes for a fast and inexpensive Mg^{2+} detection was investigated by employing PVC-based solvent polymeric membranes doped with L1-L3 uploaded on two different solid supports: Whatman 1400 filter paper (FP) and commercially available cellulose-based Color Catcher absorbent sheets (CC). Membranes of total 100 mg weight were prepared according to a common procedure^[19] (MbL.1 and MbL.2 (L=L1-L3); see the Supporting Information for more details) and their compositions are listed in Table S1.

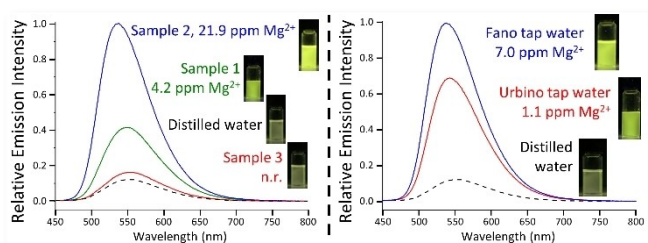


Figure 5. Real samples analysis on commercial drinking water (left) and tap water samples (right) by using L3. 37.5 μL of water samples (1.5%) were added to a DMSO solution of L3. $[\text{L3}] = 1.2 \cdot 10^{-5} \text{ mol dm}^{-3}$ DMSO, $I = 1.2 \cdot 10^{-3} \text{ mol dm}^{-3}$ NMe₄Cl. The Mg^{2+} content of each sample is reported, along with the fluorescence emission under a 365 nm UV lamp.

The membranes were doped with a lipophilic cation-exchanger (potassium tetra-*p*-chlorophenyl borate, TpCIPBK) to promote the analyte ions flux into the membrane, favoring the deprotonation of the naphtholic -OH groups of L1-L3 and the coordination of A and AE hard metals. Moreover, the small amount of lipophilic anionic TpCIPB⁻ sites stabilizes the membrane properties through keeping the overall electro-neutrality. The ligand/cation-exchanger ratios were selected based on the formation of 1:1 ligand/ Mg^{2+} complexes; variable amounts of TpCIPBK with respect to each ligand were tested (Table S1), with the highest quantity of exchanger chosen in accordance with the number of acidic groups in L1-L3 (1, 3 and 2 equiv. for L1, L2·2HCl and L3, respectively).

Arrays of sensing spots of 7 columns x 6 (A) or 5 (AE) lines size deposited on FP or CC support were prepared to test the optodes response towards A, AE and some transition metal ions (Zn^{2+} , Cd^{2+} and Pb^{2+} ; metal ions added as chloride or nitrate salts) by direct application of a drop of an aqueous solution of the analyte over the sensing spots in a concentration range from $1 \cdot 10^{-6}$ to $1 \cdot 10^{-1} \text{ mol dm}^{-3}$ (Figures 6, S10, S11).

For an optical response quantification, pictures of the optodes illuminated at 365 nm were taken with a smartphone at 10 cm distance, then the color variations were digitalized with in-house-written Matlab codes (v. 7.9, 2009, codes. The MathWorks, Inc., Natick, USA). The optodes response upon the analyte addition was converted into three main colors of the visible spectrum (red (630 nm), green (530 nm) and blue (480 nm)), according to the RGB scale, and the luminescence intensity of each sensing spot was calculated according to Equation (1):

$$I = (R + G + B)/(3 \cdot 255) \quad (1)$$

where R, G and B represent the luminescence intensities at RGB channels, while value 255 is the maximum intensity of the optical signal measured with the smartphone detector. The RGB values were extracted at the center of every single sensing spot in at least 3 replicas and evaluated after subtraction of the intensities of the spot without both the analyte and the FP or CC support background.

In accordance with the above described studies in solution, the L1-L3-based membranes showed a pronounced selectivity for Mg^{2+} over all other tested metal ions, displaying a significant naked-eye visible increase in luminescence starting from $[\text{Mg}^{2+}] = 1 \cdot 10^{-3} \text{ mol dm}^{-3}$ (Figures 6, S10, S11). Among the tested membranes, the preliminary tests have shown the highest response toward Mg^{2+} for PVC-based membranes deposited on CC solid support and for those featuring a stoichiometric amount of cation exchanger compared to the acidic functions of the ligand (MbL.2, L=L1-L3) (Figures 7 and S12). More in particular, MbL3.2, even if resulted partially luminescent itself, showed the widest linear range of luminescence response to Mg^{2+} registered as luminescence optical intensity, I , calculated as from Equation (1) (Figure 6a,b).

No influence of other A and AE were registered, except for a partial response of L1- and L3-doped membranes to high concentrations of Ca^{2+} (Figure 7).

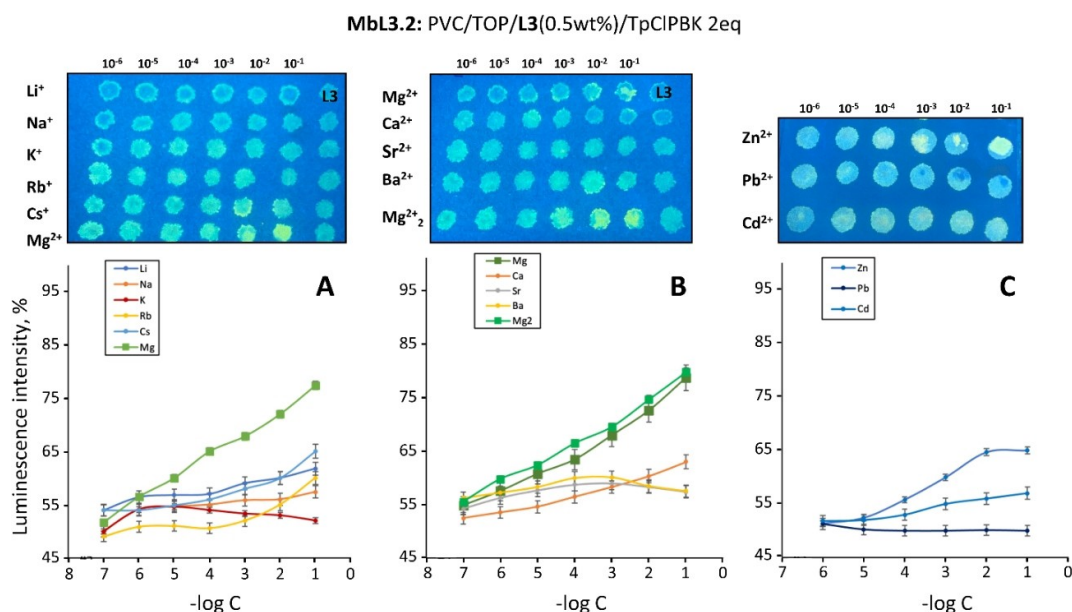


Figure 6. The response of L3-based optical sensing spot arrays to a) Alkali, b) Alkaline-Earth and c) Zn^{2+} , Pb^{2+} and Cd^{2+} metal cations, ($\lambda_{\text{ex}} = 365 \text{ nm}$). Top: photographs of sensing spots deposited on CC support; bottom: calibration curves representing the relative luminescence intensity (in %) of MbL3.2-based optode to growing concentrations ($-\log C$) of tested ions. Number of replicas: $n = 6$.

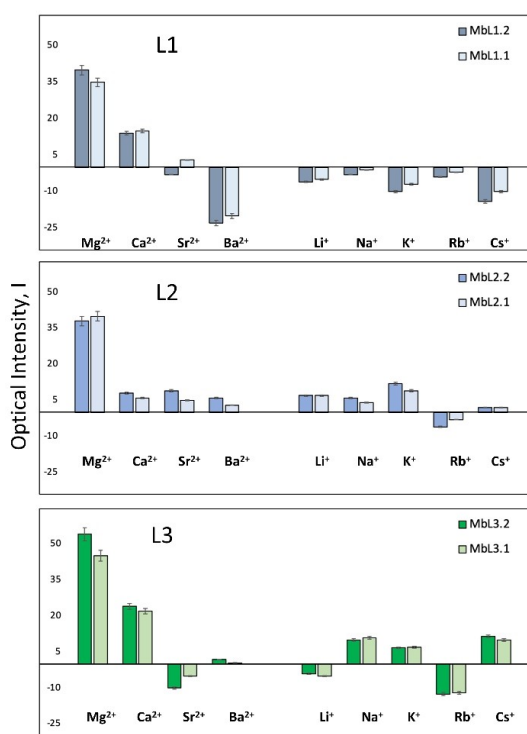


Figure 7. Optical response of L1-L3-based membranes in individual 0.01 mol dm^{-3} aqueous solutions containing A and AE. Luminescence evaluated at 365 nm .

Zn^{2+} , Cd^{2+} and Pb^{2+} were also tested, revealing a pronounced response of L1- and L2-based membranes to high concentrations of Zn^{2+} and Cd^{2+} , whereas only a modest response of L3-based optodes to Zn^{2+} was registered (Figur-

es 6c, S10c, S11c). Competition tests between $\text{Cd}^{2+}/\text{Mg}^{2+}$ or $\text{Zn}^{2+}/\text{Mg}^{2+}$ ions showed almost no influence of these interfering ions ($1 \cdot 10^{-5} \text{ mol dm}^{-3}$) on the L3-based optodes response toward Mg^{2+} (concentration range $1 \cdot 10^{-5}$ – $1 \cdot 10^{-1} \text{ mol dm}^{-3}$ for Cd^{2+} , $1 \cdot 10^{-4}$ – $1 \cdot 10^{-1} \text{ mol dm}^{-3}$ for Zn^{2+} , Figure S13).

At higher concentration ($1 \cdot 10^{-3} \text{ mol dm}^{-3}$), the interfering Cd^{2+} and Zn^{2+} ions showed more influence on the L3-based optodes response to target Mg^{2+} ions. Nevertheless, taking into account that the amount of Cd^{2+} and Zn^{2+} ions in drinking waters is commonly low and must be well controlled according to the WHO guideline for potable water,^[23] they should not interfere with the Mg^{2+} assessment by the developed optodes.

Moreover, since the pH of drinking water may vary in a quite wide range (from 5 to 8.5 pH units), the pH influence on L3-based optodes response toward Mg^{2+} ions has been investigated on different backgrounds (0.01 mol dm^{-3} MES, HEPES and PBS buffer solutions with pH 5.5, 7.5 and 8.6 respectively, and tap water with pH 8.1). The results revealed no significant pH influence on L3-based optodes luminescence response to Mg^{2+} ions in the entire tested concentration range ($1 \cdot 10^{-6}$ – $1 \cdot 10^{-1} \text{ mol dm}^{-3}$; Figure S14a) and for all the calibration curves the linear trend and the slope remain indeed the same (Figure S14b).

The disposable fluorescent sensors were hence employed for the detection of the Mg^{2+} content in solutions simulating natural waters and containing all A and AE in various concentrations (10^{-5} , 10^{-4} , $10^{-3} \text{ mol dm}^{-3}$) as far as in mineral waters. Disposable CC strips (approximately $0.9 \times 3 \text{ cm}$ size) with deposited a small sensor array formed by four sensing membranes (MbL1.2, MbL2.2, MbL3.1 and MbL3.2) replicated in two spots, were employed in these analyses (Figure S15a). A clear difference in the optical luminescence response of the sensor array in multicomponent model solutions in the presence of Mg^{2+} was observed (Figure S15a). Moreover, the

application of a PCA analysis to the numerical outputs of sensor array luminescence response in terms of RGB intensities permitted to clearly identify all multi-component model solutions in the presence and absence of Mg^{2+} ions ($1 \cdot 10^{-2} \text{ mol dm}^{-3}$, Figure S15b).

Finally, the performance of the most promising MbL3.2 membrane, preliminarily calibrated in individual solutions of Mg^{2+} (10^{-6} – $10^{-1} \text{ mol dm}^{-3}$ range), was tested for the Mg^{2+} assessment in tap, distilled and mineral waters featuring high and low magnesium content (Figure 8). Results in mineral waters were in a very good agreement with data provided by the producers, with a mean relative error (R%) lower than 5%, indicating the efficacy of the developed optical platform.

In conclusion, among three new HNBO-based ligands, L3 proved to bind Mg^{2+} in solution in a 1:1 molar ratio with a highly selective fluorescence response to Mg^{2+} also in the presence of Ca^{2+} and other Alkali and Alkaline-earth metal ions.

L3 also proved as the most promising candidate for the development of all-solid-state optodes as advantageous robust, affordable, sensitive, specific, user-friendly and equipment-free devices for magnesium detection. Both in solution and in the solid optical platform, L3 works as a probe for metal ion-induced chromo-/fluorogenic dual signaling of Mg^{2+} both in artificial and real water samples for human consumption.

Acknowledgements

Dr L. Piersanti is acknowledged for help with the synthesis of ligands L1-L3 and Ms A.R. Pierleoni for help with NMR measurements. We also acknowledge funding support from COST Action CA18202, NECTAR; MIUR, project 2017EKCS35; DISPEA ASSEGNAZIONE SICUREZZA ALIMENTARE. Open Access funding provided by Università degli Studi di Urbino Carlo Bo within the CRUI-CARE Agreement.

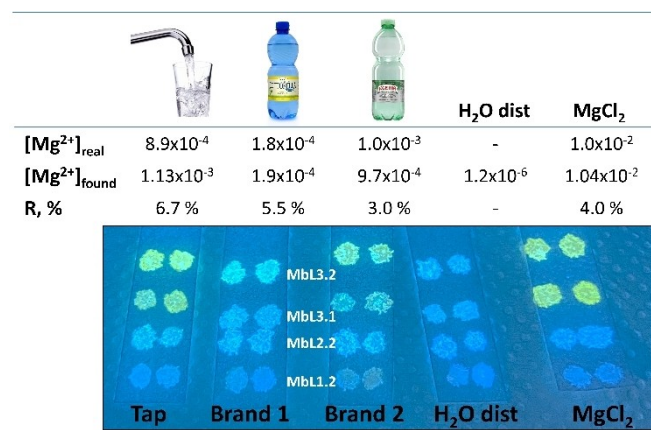


Figure 8. Real water samples analysis by using all-solid-state optodes. On the top are listed the $[\text{Mg}^{2+}]_{\text{real}}$ provided by the producer (or available on ACEA site for tap water^[24]), the $[\text{Mg}^{2+}]_{\text{found}}$ determined by MbL3.2 and the relative error, R%. Photograph taken by a smartphone upon illumination at $\lambda_{\text{ex}} = 365 \text{ nm}$ (standard laboratory UV-lamp).

Conflict of Interest

There are no conflicts to declare.

Data Availability Statement

The data that support the findings of this study are available from the corresponding author upon reasonable request.

Keywords: chemosensors · fluorescence · magnesium · natural water analysis · user-friendly detection

- [1] L. Lvova, C. G. Gonçalves, C. Di Natale, A. Legin, D. Kirsanov, R. Paolesse, *Talanta* **2018**, *179*, 430–441.
- [2] M. Algarra, C. M. Jiménez-Herrera, J. C. G. Esteves da Silva, *Crit. Rev. Anal. Chem.* **2015**, *45*, 32–40.
- [3] D. Fiorentini, C. Cappadone, G. Farruggia, C. Prata, *Nutrients* **2021**, *13*, 1136.
- [4] T. S. Lazarou, D. Buccella, *Curr. Opin. Chem. Biol.* **2020**, *57*, 27–33.
- [5] M. Liu, X. Yu, M. Li, N. Liao, A. Bi, Y. Jiang, S. Liu, Z. Gong, W. Zeng, *RSC Adv.* **2018**, *8*, 12573–12587.
- [6] P. S. Hariharan, S. P. Anthony, *RSC Adv.* **2014**, *40*, 41565–41571.
- [7] J. Yin, Y. Hu, J. Yoon, *Chem. Soc. Rev.* **2015**, *44*, 4619–4644.
- [8] H. Komatsu, N. Iwasawa, D. Citterio, Y. Suzuki, T. Kubota, K. Tokuno, Y. Kitamura, K. Oka, K. Suzuki, *J. Am. Chem. Soc.* **2004**, *126*, 16353–16360.
- [9] E. R. H. Walter, C. Hogg, D. Parker, J. A. Gareth Williams, *Coord. Chem. Rev.* **2021**, *428*, 213622.
- [10] G. Picone, C. Cappadone, G. Farruggia, E. Malucelli, S. Iotti, *Magnes. Res.* **2020**, *33*, 1–11.
- [11] Y. Li, J. Wu, X. Jin, J. Wang, S. Han, W. Wu, J. Xu, W. Liu, X. Yao, Y. Tang, *Dalton Trans.* **2014**, *43*, 1881–1887.
- [12] S. Amatori, G. Ambrosi, M. Fanelli, M. Formica, V. Fusi, L. Giorgi, E. Macedi, M. Micheloni, P. Paoli, P. Rossi, *Chem. A Eur. J.* **2014**, *20*, 11048–11057.
- [13] M. Patil, K. Keshav, M. K. Kumawat, S. Bothra, S. K. Sahoo, R. Srivastava, J. Rajput, R. Bendre, A. Kuwar, *J. Photochem. Photobiol. A* **2018**, *364*, 758–763.
- [14] L. Li, S. Yun, Z. Yuan-Hui, M. Lan, Z. Xi, C. Redshaw, W. Gang, *Sens. Actuators B* **2016**, *226*, 279–288.
- [15] S. H. Mashraqui, S. Sundaram, A. C. Bhasikuttan, S. Kapoor, A. V. Sapre, *Sens. Actuators B* **2007**, *122*, 347–350.
- [16] Y. Li, M. Y. Chi, *J. Am. Chem. Soc.* **2005**, *127*, 3527–3530.
- [17] E. Arunkumar, P. Chithra, A. Ajayaghosh, *J. Am. Chem. Soc.* **2004**, *126*, 6590–6598.
- [18] V. N. Tuan, T. D. Dinh, W. Zhang, A. M. Khattak, A. T. Le, I. A. Saeed, W. Gao, M. Wang, *RSC Adv.* **2021**, *11*, 11177–11191.
- [19] A. Garau, L. Lvova, E. Macedi, G. Ambrosi, M. C. Aragoni, M. Arca, C. Caltagirone, S. J. Coles, M. Formica, V. Fusi, L. Giorgi, F. Isaia, V. Lippolis, J. B. Orton, R. Paolesse, *New J. Chem.* **2020**, *44*, 20834–20852.
- [20] J. E. Kwon, S. Lee, Y. You, K.-H. Baek, K. Ohkubo, J. Cho, S. Fukuzumi, I. Shin, S. Young Park, W. Nam, *Inorg. Chem.* **2012**, *51*, 8760–8774.
- [21] A. C. Sedgwick, L. Wu, H. Han, S. D. Bull, X. He, T. D. James, J. L. Sessler, **2018**, 8842–8880.
- [22] A. Shrivastava, V. B. Gupta, *Chronicles Young Sci.* **2011**, *2*, 21–25.
- [23] WHO, Ed., *Guidelines for Drinking-Water Quality, 4th Edition, Incorporating the 1st Addendum*, Geneva, **2017**.
- [24] “Acea Ato 2, la mappa della qualità dell’acqua - Gruppo Acea,” can be found under <https://www.gruppo.aceaital-servizio-delle-persone/acqua/aceaital-2/la-qualita-della-tua-acqua>, n.d.

Manuscript received: April 7, 2022

Accepted manuscript online: May 27, 2022

Version of record online: July 8, 2022